Applied Catalysis B: Environmental 111–112 (2012) 303–308

Contents lists available at SciVerse ScienceDirect

Applied Catalysis B: Environmental

journal homepage: www.elsevier.com/locate/apcatb

Enhanced photocatalytic degradation of methylene blue under visible irradiation on graphene@TiO_2 dyade structure

Donglin Zhao, Guodong Sheng, Changlun Chen*, Xiangke Wang*

Key Laboratory of Novel Thin Film Solar Cells, Institute of Plasma Physics, Chinese Academy of Sciences, P.O. Box 1126, Hefei 230031, PR China

ARTICLE INFO

Article history:
Received 23 July 2011
Received in revised form
21 September 2011
Accepted 4 October 2011
Available online 12 October 2011

Keywords:
Graphene
Photocatalysis
TiO_2
Degradation

ABSTRACT

Electron–hole recombination limits the efficiency of TiO_2. We have investigated the efficacy with which the graphene@TiO_2 "dyade"-like structure reduced charge recombination and enhanced reactivity. A visible-light photocatalysis of graphene@TiO_2 "dyade"-like structure was synthesized, and photocatalytic degradation of organic compounds over the UV and visible-light spectrum regions was investigated. The graphene@TiO_2 had anatase phase and was able to absorb a high amount of photo energy in the visible-light region, driving effectively photochemical degradation reactions. There were more •OH radicals produced by the graphene@TiO_2 (1:3) than by pure TiO_2 under UV and visible-light irradiation. Graphene can enhance the photocatalytic activity of TiO_2 in two aspects, namely, e^- transportation and adsorption. This work provides new insight into the fabrication of graphene@TiO_2 as a high performance visible-light photocatalyst and facilitates its application in photocatalytic degradation of organic compounds.

1. Introduction

The photocatalytic degradation of organic compounds has attracted much attention due to its potential to purify wastewater that is discharged from industry and households [1]. Because of its low toxicity, abundance, high photostability, and high efficiency, titanium dioxide (TiO_2) has been widely used for solar energy conversion and pollutant degradation [2–5]. However, the application of pure TiO_2 is limited, because it requires ultraviolet (UV) light, which makes up only a small fraction (<4%) of the total solar spectrum reaching the surface of the earth. Therefore, over the past few years, considerable efforts have been directed towards the improvement of the photocatalytic efficiency of TiO_2 in the visible-light region [6,7]. Heterogeneous photocatalysts offer great potential for converting photon energy into chemical energy and therefore decomposing organic contaminants. A typical example is the TiO_2-based photocatalytic detoxification of air and water for environmental remediation [8,9]. However, there are still many challenges that are yet to be met before these photocatalysts become economically feasible. Difficulties include the enhancement of solar energy conversion and the suppression of the recombination of photogenerated electron–hole pairs. Some methods have been developed to increase the efficiency of the photocatalytic processes of TiO_2. One approach is doping, which introduces additional states in TiO_2 band gap and thereby increases visible-light absorbance. Anion doping with C, N and S ions or transition-metal cation doping is commonly used to convert TiO_2 into a visible-light photocatalyst [2,10–12]. However, the fact that the states introduced act as combining centers for electron–hole pairs as well as the thermal instability associated with doped materials gave rise to some doubts about their performance [2,11,13].

Modifying TiO_2 with a carbonaceous substance on the surface can induce visible-light responsive activity [14–18]. Various types of carbon, such as graphitic or coke-like carbon [15,16] or carbonate structural fragments bonding with TiO_2 [17,18] were proposed as the origin of the visible-light activity. Therefore, it can be inferred that nanostructure carbonaceous materials with tunable property could be used to modify TiO_2 surface to contrive visible-light responsive materials. Graphene is rapidly gaining interest from a wide spectrum of research fields owing to its remarkable properties, such as high carrier mobility (200 000 $cm^2 V^{-1} S^{-1}$) [19], great mechanical strength [20], excellent thermal [21] and electrical conductivity [22]. The sp^2-hybridized carbon atoms within an ideal graphene nanosheets are highly efficient in storing and shuttling electrons [23]. Therefore, graphene or graphene-based materials hold a great promise in applications requiring fast electron transfer, such as field emission displays (FEDs) [24], energy storage [25,26] and photocatalysis [27]. Given the conducting and semiconducting properties of graphene, it is possible that photoexcited electrons from TiO_2 are transferred to graphene to hinder electron–hole recombination and to enhance oxidative reactivity. There is however little work focusing on using tunable chemical properties of graphene to construct graphene@TiO_2 composites for visible-light driven photocatalytic or photoelectrochemical applications.

* Corresponding authors. Tel.: +86 551 559 2788; fax: +86 551 559 1310.
E-mail addresses: clchen@ipp.ac.cn (C. Chen), xkwang@ipp.ac.cn (X. Wang).

0926-3373/$ – see front matter © 2011 Elsevier B.V. All rights reserved.
doi:10.1016/j.apcatb.2011.10.012

Herein the graphene@TiO_2 visible-light responsive "dyade"-like structure was prepared by a two-step method, in which TiO_2 was first mounted on graphene sheets by hydrolysis of tetrabutyl titanate and further crystallized into anatase nanocrystal in a vacuum furnace at 700 °C. The photocatalytic degradation of methylene blue (MB) over the UV and visible-light spectra was investigated. The graphene@TiO_2 is able to absorb a high amount of photo energy in the visible-light region, driving effectively photochemical degradation reactions.

2. Experimental

All reagents were of analytical grade and were used as received. Milli-Q (Millipore, Billerica, MA, USA) water was used in all experiments.

2.1. Preparation of graphene@TiO_2

Graphene oxide was synthesized by the modified Hummer's method. Graphene oxide (1.0 g) was dispersed in a mixture solution of Milli-Q water (100 mL) and ethanol (100 mL) by ultrasonic treatment for 10 min, and then an ethanol solution of $Ti(OC_4H_9)_4$ was slowly added into the above suspension and stirred for 1 h. After that, the solvent (mixture of ethanol and water) was evaporated out at 90 °C. TiO_2-mounted graphene was calcinated in a vacuum furnace at 700 °C for 1 h. For comparison, we simultaneously prepared pure TiO_2 without graphene.

2.2. Characterization

Morphology and particle size were visualized using a JSM-6700F scanning electron microscope (SEM) and a JEM-2010 transmission electron microscope (TEM). XRD patterns were recorded in reflection mode (CuKα radiation, λ = 1.5418 Å) on a Scintag XDS-2000 diffractometer. UV–vis spectra were recorded on a Shimadzu UV-2550 spectrophotometer equipped with a Labsphere diffuse reflectance accessory. X-ray photoelectron spectroscopy (XPS) data were obtained with an ESCALab220i-XL electron spectrometer from VG Scientific using 300 W Al Kα radiation. The photoluminescence (PL) excitation and emission spectra were measured on a FL/FS 900 time-resolved fluorescence spectrometer.

2.3. Photocatalytic experiments

A 125 W mercury lamp was positioned inside a cylindrical vessel (supplementary data Fig. S1), surrounded by a circulating water jacket for cooling. The photocatalyst (50 mg) was suspended in 100 mL aqueous solution of 10 mg L^{-1} methylene blue (MB). The solution was stirred in dark for 2 h to ensure the establishment of an adsorption–desorption equilibrium. The probe was then irradiated with visible-light using cutoff filters (λ > 450, 600, and 700 nm, respectively). During the irradiation, 2 mL aliquots were removed at certain time intervals and analyzed with a Shimadzu UV-2550 spectrophotometer to measure MB concentrations.

3. Results and discussion

3.1. Characterization of graphene@TiO_2

Fig. 1 shows the morphology and inner structure of graphene@TiO_2. Scanning electron microscopy (SEM) shows spherically shaped particles with 30–40 nm diameter, and the colloidal particle diameter of graphene@TiO_2 is smaller than that of pure TiO_2 (100 nm, supplementary data Fig. S2B). Transmission electron microscopy (TEM) image (Fig. 1B) of graphene@TiO_2 shows a perfectly crystallized structure, with TiO_2 matrix being deposited on the surface of graphene. This means that the structure can be best understood as a "brick and mortar"-type 3D construction. X-ray diffraction (XRD) pattern (Fig. 1C) shows that the graphene@TiO_2 seems to be quite well crystallized, and only TiO_2 in anatase phase is identified. For the physical mixture of graphene and commercial P25 (1:3), there is obvious peak at $2\theta = 26.6^\circ$, corresponding to graphene. Whereas for the graphene@TiO_2, the peak at $2\theta = 26.6^\circ$ disappears. The "dyade"-like structure of the graphene@TiO_2 is different from the structure of the physical mixture catalyst. Selected area electron diffraction (SAED) pattern shows that crystal lattice fringes are observed in the inset of Fig. 1B originated from anatase, which is consistent with that obtained on the bulk materials with XRD. The lattice fringe spacing between two adjacent crystal planes of the particles was determined to be 0.35 nm from the HRTEM image, corresponding to the (1 0 1) lattice plane of anatase. This demonstrates that indeed graphene plays a supporting role in the formation of the crystalline phase through crystallite surface stabilization.

The information regarding the chemical and bonding environment of the graphene matrix and TiO_2 phase were ascertained using X-ray photoelectron spectroscopy (XPS, Fig. 1D–F, the survey spectra given in supplementary data Fig. S3A). The binding energies (BE) of Ti $2p_{3/2}$ and O 1s are 459.1 and 530.0 eV, respectively, which are identical to those for pure TiO_2. With respect to the XPS spectra of O 1s in Fig. 1E, four peaks at 530.4, 531.3, 532.17, and 533.77 eV have been fitted, which are ascribed to Ti–O–Ti (lattice O), C=O (and COO), Ti–OH, and C–OH (and C–O–C) species, respectively [28,29]. The main C 1s peak in Fig. 1F is dominated by elemental carbon at 284.6 eV, attributed mainly to sp^2 hybridized carbon (BE = 284.6 eV). The weak C 1s peak at 285.2 eV is attributed mainly to sp^3 hybridized carbon, and two weak peaks at 286.3 and 288.9 eV are assigned to the oxygen bound species C–O and O–C=O, respectively [30,31]. No C 1s peak at ~281 eV (Ti–C bond) [32] is observed, and the chemical environments for Ti and O are not changed, strongly suggesting that carbon atom does not directly enter into bulk TiO_2 lattice. This is not expected as many conventional C-doped TiO_2 is synthesized at temperatures higher than 600 °C [32–34]. Under crystallization conditions used herein, it is thought that TiO_2 is grafted onto the graphene layers via C–O–Ti bond, with such structure favouring the desired charge transfer upon light excitation [35]. C–O–Ti bond extends the light absorption to longer wavelengths.

Ultraviolet–visible (UV–vis) diffuse reflectance spectroscopy confirms that the graphene@TiO_2 composites can adsorb significantly more light in the 420–800 nm region as compared with pure TiO_2, P25, and the physical mixture of graphene and commercial P25 (1:3) (Fig. 2A). The TiO_2 band gap is obviously smeared out to longer wavelengths, whilst the graphene spectrum has changed, more in the visible range observed concurrently with less extinction in the infrared region. The enhancement of absorption in the visible range increases with increasing graphene ratio in graphene@TiO_2. This different behavior defines the graphene@TiO_2 as a "dyade" structure [17], where the combination of graphene and TiO_2 gives rise in synergistic properties arising from the beneficial interaction of the two. In other words, graphene and TiO_2 form a joint electronic system.

The photoluminescence, PL, emission spectrum has been widely used to investigate the efficiency of charge carrier trapping, immigration and transfer, and to understand the fate of e^-/h^+ pairs in semiconductor particles [36]. With the recombination of e^-/h^+ after a photocatalyst is irradiated, photons are emitted, resulting in the photoluminescence. This behavior is attributed to the reverse radiative deactivation from the excited-state of Ti species. In order to study the effect of graphene on the recombination of e^-/h^+ produced by TiO_2, the PL shown in Fig. 2B compares the

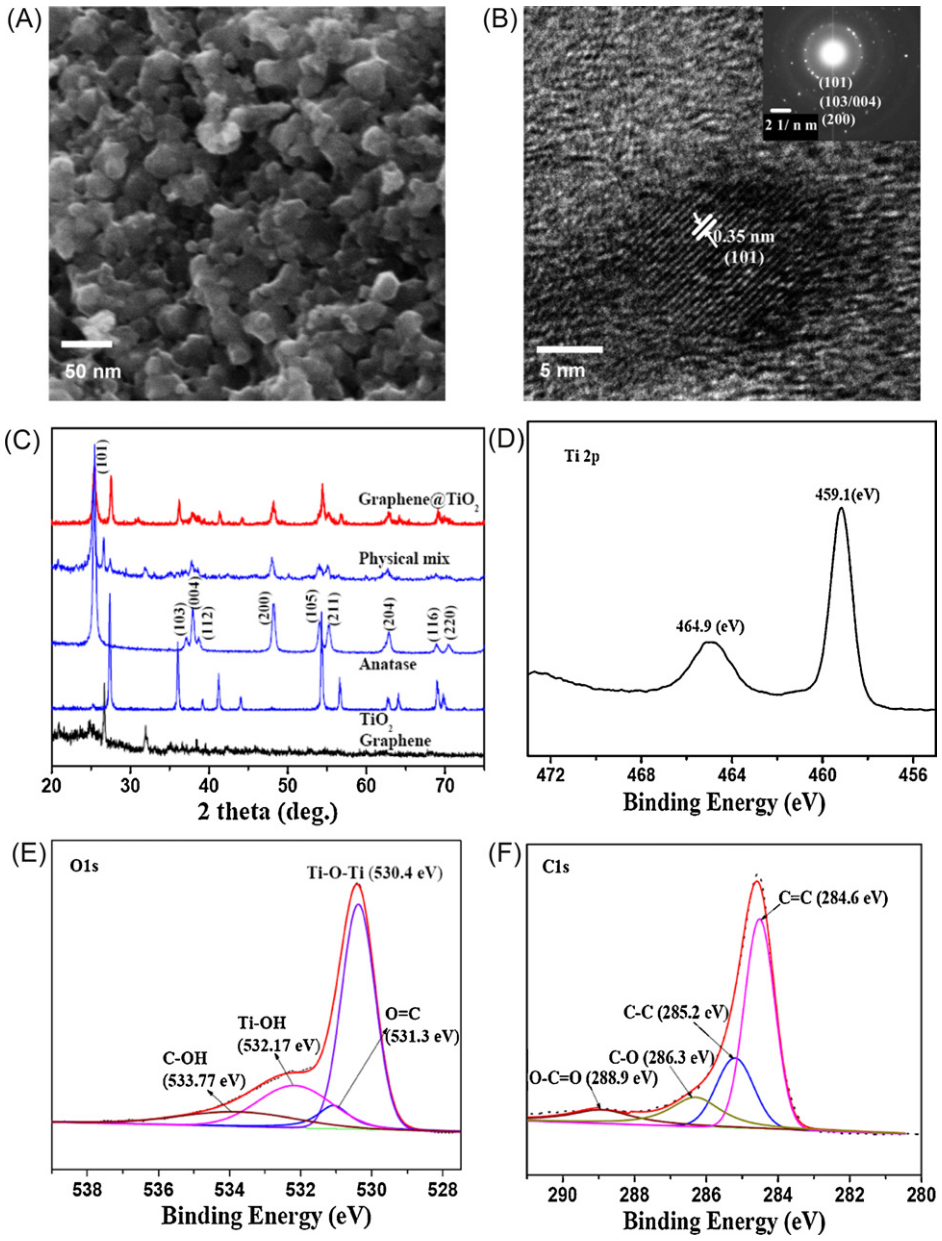

Fig. 1. SEM (A), TEM (B), XRD patterns (C), and High resolution Ti (D), O (E), and C (F) XPS of the graphene@TiO_2 dyade structure.

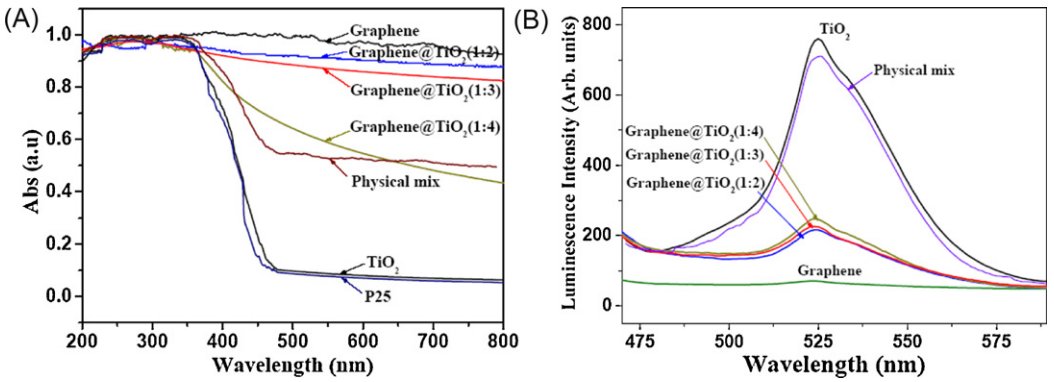

Fig. 2. (A) UV–vis diffuse reflectance spectra, and (B) PL spectra of graphene, TiO_2, P25, physical mixture of graphene and P25 (1:3), and graphene@TiO_2.

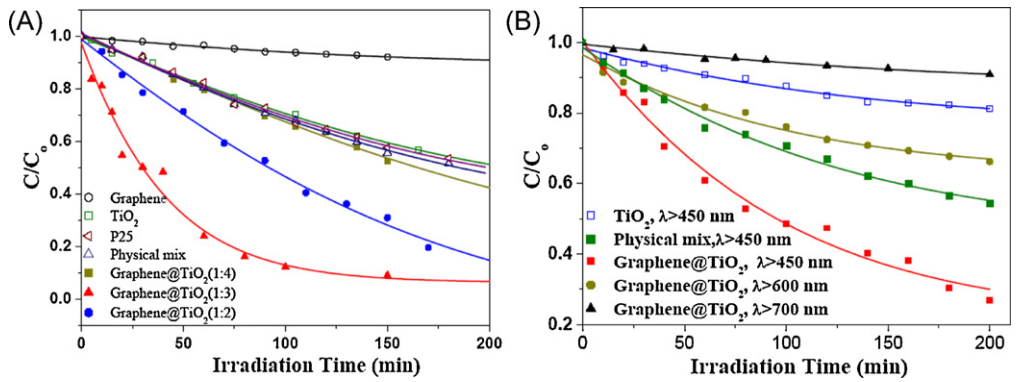

Fig. 3. Photocatalytic degradation of MB by graphene, TiO_2, P25, physical mixture of graphene and P25 (1:3), and graphene@TiO_2 under UV light (A). Photocatalytic degradation of MB by pure TiO_2, physical mixture of graphene and P25 (1:3), and graphene@TiO_2 (1:3) under visible light (filter: $\lambda > 450$, 600, and 700 nm, respectively) (B).

e^-/h^+ recombination of graphene@TiO_2 to the physical mixture of graphene and commercial P25 (1:3), TiO_2, and graphene. TiO_2 powder shows a broad PL emission band, which is similar to the results in the earlier study [37]. The emission band corresponding to the peak position of ~520 nm is for anatase powder [38]. As expected, no PL signal is observed in the range of 500–600 nm for graphene. The graphene@TiO_2 shows diminished PL intensity indicating reduced charge recombination in comparison to TiO_2 alone. This reduction increases with increasing graphene ratio in the graphene@TiO_2. Peak shifts are caused by the trapping of electrons at defect sites prior to recombination [38]. For the physical mixture of graphene and commercial P25, there is only slight PL intensity reduction, indicating the structure of "dyade"-like is important for recombination reduction.

3.2. Photodegradation of MB

The photocatalytic activities of graphene, pure TiO_2, P25, the physical mixture of graphene and commercial P25 (1:3), and the graphene@TiO_2 were measured by the photodegradation of MB as a model reaction under UV and visible-light ($\lambda > 450$, 590, and 700 nm), and the results are shown in Fig. 3A and B, respectively. The normalized temporal concentration changes (C/C_o) of MB during the photodegradation are proportional to the normalized maximum absorbance (A/A_o) and derived from the changes in MB's absorption profile ($\lambda = 633$ nm) at a given time interval. It is clear from Fig. 3A that the graphene@TiO_2 shows significant progress in the photodegradation of MB compared to graphene, pure TiO_2, P25, the physical mixture of graphene and P25 (1:3), and it also exhibits the highest efficiency at the mass ratio of graphene:TiO_2 = 1:3. Under UV light irradiation, about 88% MB is decomposed by the graphene@TiO_2 (1:3) after less than 100 min. Contrastingly, 60–70% MB still remains in the solution after the same time period for pure TiO_2, P25, the physical mixture of graphene and P25 (1:3). In addition, in the visible-light photodegradation (Fig. 3B), pure TiO_2 shows rather poor photocatalytic activity due to its limited photoresponding range and only 13% of the initial MB diminishes after more than 100 min. The photodegradation rate of the physical mixture of graphene and P25 is 30% after irradiation time of 100 min at $\lambda > 450$ nm. Whereas the graphene@TiO_2 (1:3) shows remarkable improvement in the photodegradation rate and 52% of MB is decomposed. The graphene@TiO_2 shows the highest photocatalytic activity of all compared materials under light with a wavelength larger than 450, 600, and 700 nm, respectively, thus proving that indeed a special performance is to be expected, because of the dyadic bonding between graphene and TiO_2.

3.3. Mechanism of the enhanced photocatalysis

The electron paramagnetic resonance (EPR) spin trap technique, using 5,5-dimethyl-1-pyrroline-*N*-oxide (DMPO) as the spin-trapping reagent, is well-known to be an efficient measurement method to determine •OH. Fig. 4 shows the EPR spectra of DMPO-•OH spin adducts produced in the dispersion systems of graphene, TiO_2 and graphene@TiO_2 (1:3) as easily identified by the classical 1:2:2:1 spectral signature of spin-trapped •OH. Under UV irradiation, the intensity of the 1:2:2:1 spectral signature of the DMPO-•OH spin adducts for the graphene@TiO_2 (1:3) is obviously stronger than that with TiO_2, and there is no 1:2:2:1 spectral signature of the DMPO-•OH spin adducts for graphene. Under visible-light irradiation, there is no obvious 1:2:2:1 spectral signature of the DMPO-•OH spin adducts for TiO_2, whereas, there is strong 1:2:2:1 spectral signature of the DMPO-•OH spin adducts for the graphene@TiO_2 (1:3). Therefore, the graphene@TiO_2 (1:3)

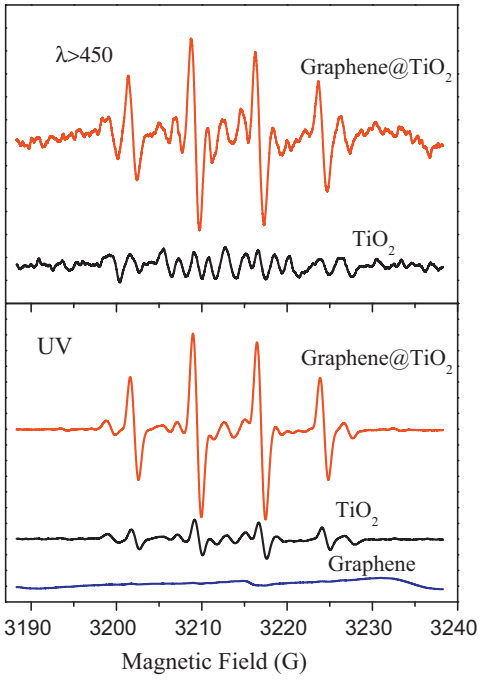

Fig. 4. The hydroxyl radical EPR spectra of graphene, pure TiO_2, and graphene@TiO_2 (1:3) formed in aqueous dispersions in a pyrex vessel containing about 20 mg sample after 2 min irradiation by UV and after 5 min irradiation by visible-light (filter: $\lambda > 450$). In the system, the concentration of DMPO is 0.4 mol L^{-1}.

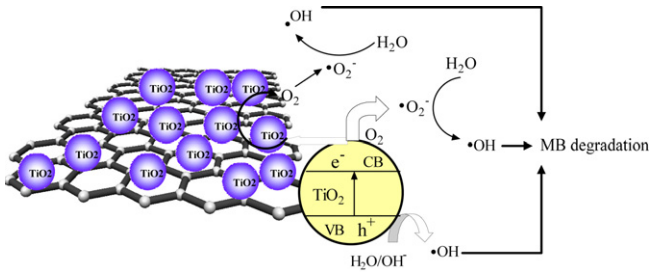

Fig. 5. The schematic illustration of mechanism of the activation of photocatalytic activity for MB by graphene@TiO_2.

is photocatalytically more active than TiO_2 because there are more •OH radicals produced by the graphene@TiO_2 (1:3) under UV and visible-light irradiation. It could be inferred that MB were eliminated mainly by means of •OH radical oxidation under UV and visible light irradiation.

The schematic mechanism illustration of the enhancement of photocatalytic activity for TiO_2 by graphene is summarized in Fig. 5. From all experimental results mentioned above, it can be proposed that graphene can enhance the photocatalytic activity of TiO_2 in two aspects, namely, e^- transportation and adsorption. It is confirmed that the graphene@TiO_2 can induce the formation of hydroxyl radical under visible-light irradiation ($\lambda > 450$ nm). However, this ability relies on the fact that the hole of the joint system is position near the TiO_2 valence band, as it needs ~2.4 V versus normal hydrogen electrode to drive the hydroxyl radical formation. This would be not possible for the usual sensitizing situation, which would fill the much less noble and therefore less reactive graphene sub-gaps. On the base of our experimental data, it is proposed that the synergistic dyade structure of graphene@TiO_2 provides access to optically active charge transfer transition. Under visible-light irradiation, electrons (e^-) are excited from the valence band (VB) to the conduction band (CB) of TiO_2, creating a change vacancy, or hole (h^+), in the CB. In the absence of graphene, most of these charges quickly recombine without doing any chemistry. Typically, only a small number of electrons (<1%) and holes are trapped and participate in photocatalytic reactions, resulting in low reactivity [39]. It has been reported that the CB position of anatase is about −4.21 eV using vacuum level as a reference, with a band gap of about 3.2 eV [40]. The work function of graphene was similar to that of graphite, ~4.6 eV, depending sensitively on the number of layers [41]. Theoretical investigations predicted that a sizable band gap of graphene was about 0.3 eV in Bernal-stacking bilayer graphene [42]. TiO_2 nanoparticles are in intimate contact with graphene. The d-orbital (CB) of TiO_2 and π-orbital of graphene match well in energy levels and have chemical bond interactions and form d–π electron orbital overlap, which can cause synergic effect. TiO_2 absorbs UV and visible light, transporting the excited-state electrons from the d-orbital (CB) of TiO_2 into the π-orbital of graphene and the excited electrons can be shuttled freely along the conducting network of graphene, and subsequently transfer to the surface to react with water and oxygen to yield hydroxyl radical, which would oxidize MB. The excited-electrons are transferred to the nanocylinder of graphene from the surface of TiO_2, allowing charge separation, stabilization, and hindered recombination. The longer-lived holes on TiO_2, then, account for the higher activity of the graphene@TiO_2 dyade structure photocatalyst. Furthermore, the adsorption ability of TiO_2 bound to graphene greatly increases due to more active sites available on the surface of graphene. Since O_2 may be adsorbed on the surface of graphene, the e^- in the graphene reacts with O_2 and finally forms •OH, which oxidizes the adsorbed MB directly on the surface. The routes of formation of •OH and the photodegradation of MB can be described as follows:

$$TiO_2 + h\nu \rightarrow (e^-_{CB}) + (h^+_{VB}) \rightarrow \text{Graphene}\ (e^-) + h^+ \quad (1)$$

$$TiO_2(h^+_{VB}) + OH^-_{ads} \rightarrow {}^\bullet OH + TiO_2 \quad (2)$$

$$TiO_2(e^-_{CB}) + O_{2ads} \rightarrow {}^\bullet O_2{}^- + TiO_2 \xrightarrow{H_2O} {}^\bullet OH + TiO_2 \quad (3)$$

$$\text{Graphene}\ (e^-) + O_{2ads} \rightarrow {}^\bullet O_2{}^- + \text{Graphene} \xrightarrow{H_2O} {}^\bullet OH + \text{Graphene} \quad (4)$$

$$MB_{ads} + {}^\bullet OH \rightarrow \text{Degraded products} \quad (5)$$

The amount of •OH formed in the system with TiO_2 bound to graphene is more than that with TiO_2 alone as a photocatalyst. Moreover, MB molecules can transfer from solution to the catalyst's surface and be adsorbed with offset face-to-face orientation via π–π conjugation between MB and aromatic regions of the graphene, and therefore, the adsorptivity of MB on graphene increases compared to that of MB on bare TiO_2. Therefore, graphene@TiO_2 has higher efficiency in photodegradation of MB compared to TiO_2 alone as a photocatalyst.

4. Conclusion

A novel graphene@TiO_2 visible-light responsive "dyade"-like structure is synthesized. The graphene@TiO_2 has anatase phase and is able to absorb a high amount of photoenergy in the visible-light region, driving effectively photochemical degradation reactions. Photochemical characterization of the graphene@TiO_2 confirmed that the origin of photocatalytic activity under visible light is due to a direct optical charge transition involving both TiO_2 and graphene, keeping the high reactivity of the photogenerated electron and hole. The results of this research highlighted new insight into the fabrication of the graphene@TiO_2 as a high performance visible-light responsive catalyst and facilitates its application in environmental protection issues. Our findings are relevant and important for the use of the graphene@TiO_2 in photocatalytic degradation of organic compounds.

Acknowledgements

Authors D.L. Zhao and G.D. Sheng contributed equally to this paper. Financial support from the National Natural Science Foundation of China (21071147; 21077107), and the 973 project of MOST (2011CB933700) are acknowledged.

Appendix A. Supplementary data

Supplementary data associated with this article can be found, in the online version, at doi:10.1016/j.apcatb.2011.10.012.

References

[1] M. Kaneko, I. Okura, in: M. Kaneko, I. Okura (Eds.), Photocatalysis, Kohdansha-Springer, Tokyo, Japan, 2002.
[2] R. Asahi, T. Morikawa, T. Ohwaki, K. Aoki, Y. Taga, Science 293 (2001) 269–271.
[3] M.A. Fox, M.T. Dulay, Chem. Rev. 93 (1993) 341–357.
[4] M.R. Hoffmann, S.T. Martin, W. Choi, D.W. Bahnemann, Chem. Rev. 95 (1995) 69.
[5] S.U.M. Khan, M. Al-Shahry, W.B. Ingler, Science 297 (2002) 2243–2245.
[6] K. Vinodgopal, D.E. Wynkoop, P.V. Kamat, Environ. Sci. Technol. 30 (1996) 1660–1666.
[7] D. Zhao, C.C. Chen, Y. Wang, W.H. Ma, J.C. Zhao, T. Rajh, L. Zang, Environ. Sci. Technol. 42 (2008) 308–314.
[8] J.C. Crittenden, Y. Zhang, D.W. Hand, D.L. Perram, Water Environ. Res. 68 (1996) 270–2778.
[9] N.V. Muradov, Sol. Energy 52 (1994) 283–288.

[10] J.C. Zhao, T.X. Wu, K.Q. Wu, K. Okawa, H. Hidaka, N. Serpone, Environ. Sci. Technol. 32 (1998) 2245–2394.
[11] S. Sakthivel, H. Kisch, Angew. Chem. Int. Ed. 42 (2003) 4908–4911.
[12] Y.F. Wang, D. Zhao, W.H. Ma, C.C. Chen, J.C. Zhao, Environ. Sci. Technol. 42 (2008) 6173–6178.
[13] W. Choi, J. Phys. Chem. 98 (1998) 13669–13679.
[14] C. Chen, M. Long, H. Zeng, W. Cai, B. Zhou, J. Zhang, Y. Wu, D. Ding, D. Wu, J. Mol. Catal. A 314 (2009) 35–41.
[15] C. Lettmann, K. Hildenbrand, H. Kisch, W. Macyk, W.F. Maier, Appl. Catal., B 32 (2001) 215–227.
[16] L.W. Zhang, H.B. Fu, Y.F. Zhu, Adv. Funct. Mater. 18 (2008) 2180–2189.
[17] L. Zhao, X. Chen, X. Wang, Y. Zhang, W. Wei, Y. Sun, M. Antonietti, M.M. Titirici, Adv. Mater. 22 (2010) 3317–3321.
[18] P. Zabek, J. Eberl, H. Kisch, Photochem. Photobiol. Sci. 8 (2009) 264–269.
[19] K.I. Bolotin, K.J. Sikes, Z. Jiang, M. Klima, G. Fudenberg, J. Hone, P. Kim, H.L. Stormer, Solid State Commun. 146 (2008) 351–355.
[20] C. Lee, X. Wei, J.W. Kysar, J. Hone, Science 321 (2008) 385–388.
[21] A.A. Balandin, S. Ghosh, W. Bao, I. Calizo, D. Teweldebrhan, F. Miao, C.N. Lau, Nano Lett. 8 (2008) 902–907.
[22] S. Park, R.S. Ruoff, Nat. Nanotechnol. 4 (2009) 217–224.
[23] S. Stankovich, D.A. Dikin, G.H.B. Dommett, K.M. Kohlhaas, E.J. Zimney, E.A. Stach, R.D. Piner, S.T. Nguyen, R.S. Ruoff, Nature 442 (2006) 282–286.
[24] H. Yoon, K. Seo, N. Bagkar, J. In, J. Park, J. Kim, B. Kim, Adv. Mater. 21 (2009) 4979–4982.
[25] G.K. Dimitrakakis, E. Tylianakis, G.E. Froudakis, Nano Lett. 8 (2008) 3166–3170.
[26] L.L. Zhang, R. Zhou, X.S. Zhao, J. Mater. Chem. 20 (2010) 5983–5992.
[27] Z. Xiong, L.L. Zhang, J. Ma, X.S. Zhao, Chem. Commun. 46 (2010) 6099–6101.
[28] G.M. An, W.H. Ma, Z.Y. Sun, Z.M. Liu, B.X. Han, S.D. Miao, Z.J. Miao, K.L. Ding, Carbon 45 (2007) 795–1801.
[29] N.P. Zschoerper, V. Katzenmaier, U. Vohrer, M. Haupt, C. Oehr, T. Hirth, Carbon 47 (2007) 2174–2185.
[30] E. Papirer, R. Lacroix, J.-B. Donnet, G. Nansé, P. Fioux, Carbon 33 (1995) 63–72.
[31] W.J. Ren, Z.H. Ai, F.L. Jia, L.Z. Zhang, X.X. Fan, Z.G. Zou, Appl. Catal. B: Environ. 69 (2007) 138–144.
[32] H. Irie, Y. Watanabe, K. Hashimoto, Chem. Lett. 32 (2003) 772–773.
[33] T. Tsumura, N. Kojitani, I. Izumi, N. Iwashita, M. Toyoda, M. Inagaki, J. Mater. Chem. 12 (2002) 1391–1396.
[34] B. Tryba, A.W. Morawski, T. Tsumura, M. Toyoda, M. Inagaki, J. Photochem. Photobiol. A 167 (2004) 127–135.
[35] M. Niederberger, G. Garnweitner, F. Krumeich, R. Nesper, H. Colfen, M. Antonietti, Chem. Mater. 16 (2004) 1202–1208.
[36] J.G. Yu, H.G. Yu, B. Cheng, X.J. Zhao, J.C. Yu, W.K. Ho, J. Phys. Chem. B 107 (2003) 13871–13879.
[37] X.Z. Li, F.B. Li, C.L. Yang, W.K. Ge, J. Photochem. Photobiol. A: Chem. 141 (2001) 209–217.
[38] K. Fujihara, S. Izumi, T. Ohno, M. Matsumura, J. Photochem. Photobiol. A: Chem. 132 (2000) 99–104.
[39] G. Li, K.A. Gray, Chem. Phys. 339 (2007) 173–185.
[40] Y. Xu, M.A.A. Schoonen, Am. Mineral. 85 (2000) 543–556.
[41] Y.J. Yu, Y. Zhao, S. Ryu, L.E. Brus, K.S. Kim, P. Kim, Nano Lett. 9 (2009) 3430–3434.
[42] F. Xia, D.B. Farmer, Y. Lin, P. Avouris, Nano Lett. 10 (2010) 715–718.